flatter than the ρ. See R. J. N. Phillips and W. Rarita, Phys. Lett. $\underline{19}$, 598 (1965), and Ref. 10.

[10]R. D. Mathews, Nucl. Phys. $\underline{B11}$, 339 (1969).

[11]M. Krammer and U. Maor, Nucl. Phys. $\underline{B13}$, 651 (1969).

[12]The value of X for 3.5 GeV/c was taken from Ref. 2. Reference 2 does not quote a total cross section and we calculate it in the same manner as for the data of this experiment.

[13]Particle Data Group, Phys. Lett. $\underline{39B}$, 1 (1972).

[14]The original distributions were plotted vs $t' = t - t_{min}$. In Fig. 5 the distributions are shifted by a t_{min} calculated for a nominal η and Δ^{++} of masses 0.55 and 1.23 GeV, respectively.

[15]L. Stodolsky and J. J. Sakurai, Phys. Rev. Lett. $\underline{11}$, 90 (1963).

[16]Other approaches have yielded this same result. See, e.g., R. Dashen and S. Frautschi, Phys. Rev. $\underline{152}$, 1450 (1966).

[17]We quote the joint error between α_0 and α', $\delta\alpha_0\delta\alpha'$, since the two quantities are highly ($\sim 90\%$) correlated. Proper numerical comparisons of our result to other trajectories must include this joint error.

[18]The point at $t = -0.075$ (GeV/c)^2 is not used since it is near kinematic threshold at the lower momenta. The

point at $t = -1.05$ (GeV/c)^2 is not used because there are no data at this t value at 5 and 8 GeV/c.

[19]We adopt a standard notation $LL'2J$, where L refers to the angular momentum of the initial state, L' to the final state, and J is the total spin. Since all resonances discussed here have isospin $I = \frac{3}{2}$, we delete the usual reference to that quantity. When referring to the elastic channel, we delete L'.

[20]U. Mehtani, S. Y. Fung, A. Kernan, T. L. Schalk, Y. Williamson, R. W. Birge, G. E. Kalmus, and W. Michael. Phys. Rev. Lett. $\underline{29}$, 1634 (1972).

[21]U. Mehtani, University of Calif. Riverside Report No. UCR 34 P107-132, 1971 (unpublished).

[22]At a typical momentum in this low-energy region, the number of $\eta\Delta$ events (with the decay $\eta \to \pi^+\pi^-\pi^0$) is only $\sim 1/15$ of the number of $\pi^0\Delta$ events.

[23]G. Gidal, G. Borreani, D. Grether, F. Lott, R. W. Birge, S. Y. Fung, W. Jackson, and R. Poe, Phys. Rev. Lett. $\underline{23}$, 994 (1969). From Fig. 1 of this reference we take the normalization of the $P_{lab}^{-1.6}$ behavior as 0.6 mb at 3 GeV/c.

[24]J. J. de Swart, Rev. Mod. Phys. $\underline{35}$, 916 (1963).

[25]G. Trilling, Nucl. Phys. $\underline{B40}$, 13 (1972).

[26]R. G. Roberts, Ann. Phys. (N.Y.) $\underline{44}$, 325 (1967).

Study of $K^-p \to \Sigma\pi\pi$ in the Region of the $\Lambda(1520)$ *

T. S. Mast, R. O. Bangerter, M. Alston-Garnjost, A. Barbaro-Galtieri,

L. K. Gershwin, F. T. Solmitz, and R. D. Tripp

Lawrence Berkeley Laboratory, University of California, Berkeley, California 94720
(Received 28 July 1972)

The reactions $K^-p \to \Sigma^+\pi^-\pi^0$, $\Sigma^-\pi^+\pi^0$, and $\Sigma^0\pi^+\pi^-$ have been analyzed in the region of the $\Lambda(1520)$. The data are consistent with the dominance of the reaction sequence $K^-p \to \Lambda(1520) \to \Sigma(1385)\pi \to \Sigma\pi\pi$. The same sequence of resonance production and decay has been previously found to lead to the $\Lambda\pi\pi$ final state. Fits to the cross sections yield branching fractions for $\Lambda(1520) \to \Sigma^+\pi^-\pi^0$, $\Sigma^-\pi^+\pi^0$, and $\Sigma^0\pi^+\pi^-$ of 0.0034 ± 0.0004, 0.0024 ± 0.0003, and 0.0027 ± 0.0003, respectively. A comparison of the $\Sigma\pi\pi$ and $\Lambda\pi\pi$ cross sections yields a branching ratio $\Gamma[\Sigma(1385) \to \Sigma\pi]/\Gamma[\Sigma(1385) \to \Lambda\pi] = 0.18 \pm 0.04$.

I. INTRODUCTION

In the region of 400-MeV/c incident K^- momentum the predominant structure in the $\bar{K}N$ reaction channel is the $\Lambda(1520)$. We have previously reported on a detailed analysis of the reaction $K^-p \to \Lambda\pi^+\pi^-$ in this region.[1] This reaction was observed to proceed as

$$K^-p \to \Lambda(1520) \to \Sigma(1385)\pi \to \Lambda\pi^+\pi^- . \tag{1}$$

We describe here the analysis of about 1900 events of the type $K^-p \to \Sigma\pi\pi$ from the same bubble-chamber exposure. This final state is found to be sim-

ilar in many respects to $\Lambda\pi\pi$. In Sec. II we describe the separation of $\Sigma\pi\pi$ events in three different charge channels. A description of the investigation of event loss and possible contaminations is given. The series of cuts and weights used to account for event loss is explained. Section III presents cross sections and angular distributions. The cross sections allow a measurement of the branching fraction of the $\Lambda(1520)$ into $\Sigma^+\pi^-\pi^0$, $\Sigma^-\pi^+\pi^0$, and $\Sigma^0\pi^+\pi^-$. The angular distributions indicate the dominance of the reaction sequence

$$K^-p \to \Lambda(1520) \to \Sigma(1385)\pi \to \Sigma\pi\pi . \tag{2}$$

In Sec. IV a comparison is made between the cross sections for the $\Sigma\pi\pi$ and $\Lambda\pi\pi$ final states. This yields branching fractions for $\Sigma(1385)$.

II. EXPERIMENTAL PROCEDURES

An exposure of the Berkeley 25-in. hydrogen bubble chamber to a K^- beam has yielded 1.3×10^6 pictures with 11 events/μb. The incident momentum ranges from 270 to 470 MeV/c. Most of the path length is close to 395 MeV/c, the incident momentum required to form the $\Lambda(1520)$.

The film was scanned for all track topologies, including those resulting from the following reactions:

$$K^-p \to \Sigma^+\pi^-, \quad \Sigma^+ \to p\pi^0 \text{ or } n\pi^+, \tag{3a}$$

$$\to \Sigma^+\pi^-\pi^0, \tag{3b}$$

$$\to \Sigma^-\pi^+, \quad \Sigma^- \to n\pi^-, \tag{4a}$$

$$\to \Sigma^-\pi^+\pi^0, \tag{4b}$$

$$\to \Lambda\pi^+\pi^-, \quad \Lambda \to p\pi^-, \tag{5a}$$

$$\to \Sigma^0\pi^+\pi^-, \quad \Sigma^0 \to \Lambda\gamma, \quad \Lambda \to p\pi^-. \tag{5b}$$

All of the film was scanned once; 38% was scanned twice; and 7% was scanned three times. All events within a restricted fiducial volume were measured and the track reconstruction and kinematic fitting were performed with the programs TVGP and SQUAW. Table I shows the numbers of events which passed a kinematic fit with a confidence level greater than 1% for at least one of the six reactions above.

There are two general problems associated with obtaining a usable sample of $\Sigma\pi\pi$ events. The first involves scanning efficiencies and losses in the measuring and fitting processes. The second problem is the possible contamination of the $\Sigma\pi\pi$ events by channels with the same topology. A detailed analysis of the detection efficiencies has been made and a series of cuts and weights

has been applied to the events to account for loss due to scanning and measuring. At these incident momenta the kinematics of the $\Sigma\pi\pi$ are sufficiently different from the kinematics of other channels that the problem of ambiguities is minor.

A. Detection Efficiencies

Losses in measurement and fitting have been reduced to about 5% by repeated remeasurement of events failing to give satisfactory fits to any possible reaction hypothesis. Roughly 2% are unmeasurable because of obscured vertices or extremely short tracks. Some of the remaining 3% of the "charged Σ events" are not Σ events at all but K^-p scatterings followed by K^- decay or pp scattering with an invisible proton. However, most of the 3% simply fail to give a fit with a confidence level greater than 1% and are rejected. This excess of events having a low confidence level is not unexpected in bubble-chamber experiments, since the scattering processes that contribute to the uncertainties in track measurement have larger tails than the Gaussian distributions assumed in calculating the confidence level.

The $\Sigma^\pm\pi^\mp\pi^0$ events have a slightly higher failure rate on the first measurement than the $\Sigma^\pm\pi^\mp$ events. However, the events have been remeasured a sufficient number of times so that all channels have the same 5% loss rate.

We require minimum projected decay lengths of 0.15 cm and 0.25 cm for the $\Sigma^\pm$ and Λ hyperons, respectively. We also require the angle between the $\Sigma^\pm$ and its charged decay product to be larger than either 8° in projection or 40° in space. The length of the charged decay track must be greater than either 0.5 cm in projection or 2.5 cm in space. For the Λ events we require the decay proton to be longer than 0.3 cm.

The events satisfying these criteria are weighted to account for those rejected and for losses

TABLE I. Numbers of events passing selection criteria.

Final state		Events passing fit criteria	Events remaining after cuts	Weighted events
$\Sigma^+\pi^-$	$\Sigma^+ \to p\pi^0$	40 127	24 751	55 204
	$\Sigma^+ \to n\pi^+$	44 871	36 682	54 715
$\Sigma^-\pi^-$		60 756	51 828	71 404
$\Lambda\pi^+\pi^-$		10 292	9 223	11 361
$\Sigma^+\pi^-\pi^0$	$\Sigma^+ \to p\pi^0$	390	306	519
	$\Sigma^+ \to n\pi^+$	403	330	454
$\Sigma^-\pi^+\pi^0$		509	461	564
$\Sigma^0\pi^+\pi^-$		338	313	365

due to escape from the chamber fiducial volume. Weights are also applied to correct for scanning losses that occur when the projected length of the Σ track is less than 0.75 cm or when the edge of the Λ decay plane faces the cameras. Additional weights for scanning inefficiencies of 3% for the $\Sigma^{\pm}$ events and 4% for the Σ^0 events are applied. These topological scanning inefficiencies are obtained from the topologically similar $\Sigma\pi$ and $\Lambda\pi\pi$ events by comparing the three scans, using a method similar to that of Hildebrand and Derenzo.[2] Table I shows the numbers of events surviving the cuts and the total numbers of events.

B. Contamination

Since the $\Sigma^{\mp}\pi^{\pm}$ events are about 100 times more numerous than the $\Sigma^{\mp}\pi^{\pm}\pi^0$ events, contamination of the $\Sigma^{\mp}\pi^{\pm}\pi^0$ channels might be expected to be a problem. In fact only about 4% of the events that give an adequate 1-constraint fit to $\Sigma^-\pi^+\pi^0$ (confidence level 1%) also give a 4-constraint[3] (confidence level 10^{-5}) fit to $\Sigma^-\pi^+$. Similarly only 9% of the events that fit $\Sigma^+\pi^-\pi^0$ also fit $\Sigma^+\pi^-$. However, most of these events are not truly ambiguous and can be easily separated on the basis of confidence-level ratios. We calculate that the contamination from $\Sigma\pi$ events is less than 1% for all event types.

We have also investigated the possibility of contamination by $\Sigma\pi\gamma$ events and $\Sigma\pi$ events that are so badly measured that they fail to give a fit to the $\Sigma\pi$ hypothesis. This was done by comparing the missing-neutral-mass distribution for the $\Sigma^{\mp}\pi^{\pm}\pi^0$ events to a Monte Carlo prediction. From this comparison we conclude that the contamination from these sources is negligible.

Finally, we note that the confidence-level distributions for $\Sigma^{\mp}\pi^{\pm}\pi^0$ are very nearly flat, and in particular show no peaking near the lower limit of 1% as might be expected if significant contamination were present.

The $\Sigma^0\pi^+\pi^-$ channel is very cleanly separated. The 7-constraint fits to $\Lambda\pi^+\pi^-$ and 5-constraint fits to $\Sigma^0\pi^+\pi^-$ yielded fewer than 10 events that fit both hypotheses. Subsequent reexamination of these events showed them to be mismeasured.

III. DATA

The total cross sections for the $\Sigma\pi\pi$ final states (Fig. 1) were determined by comparing the ratios of weighted events $N(\Sigma^{\pm}\pi^{\mp}\pi^0)/N(\Sigma^{\pm}\pi^{\mp})$ and $N(\Sigma^0\pi^+\pi^-)/N(\Lambda\pi^+\pi^-)$ to the known cross sections for the $\Sigma^{\pm}\pi^{\mp}$ and $\Lambda\pi^+\pi^-$ final states. For convenience the latter cross sections were obtained from smooth curves coming from our high-sta-

tistics partial-wave analysis of the major final states in this region. The inputs to this partial-wave analysis are measured cross sections, angular distributions, and polarizations from this same bubble-chamber exposure. The $\Sigma^{\pm}\pi^{\mp}$ and $\Lambda\pi^+\pi^-$ cross sections are measured to a precision of about 5%, and the smooth predictions are in good agreement with these. Since the results of this partial-wave analysis are not final, an additional uncertainty of 5% has been incorporat-
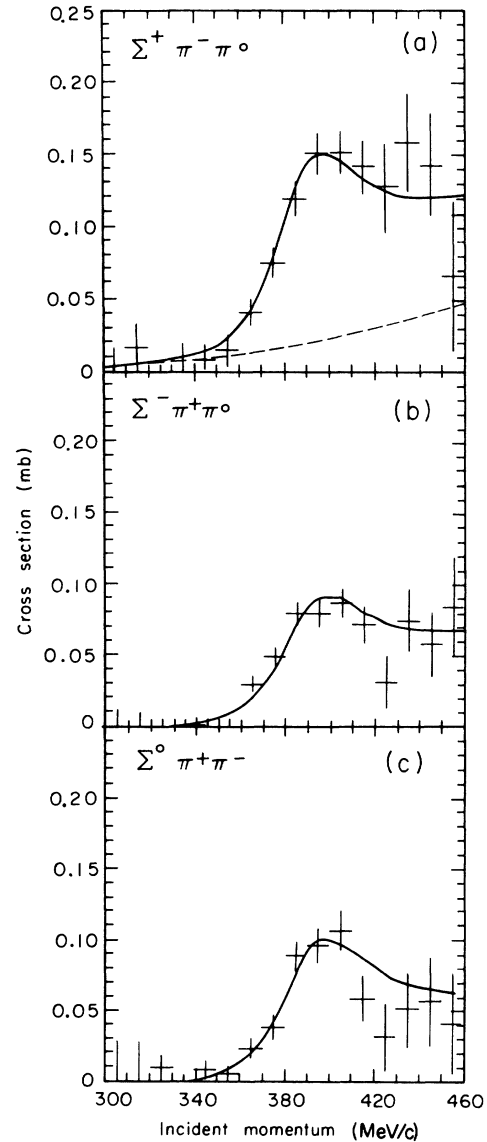

FIG. 1. Cross sections in mb as a function of incident K^- momentum (MeV/c) for the final states (a) $\Sigma^+\pi^-\pi^0$, (b) $\Sigma^-\pi^+\pi^0$, and (c) $\Sigma^0\pi^+\pi^-$. The curves are the results of the χ^2 fits described in the text. The dashed line in Fig. 1(a) is the background contribution.

ed in the estimation of the errors.

The $\Sigma\pi\pi$ thresholds lie between 220 and 255 MeV/c. Near 300 MeV/c the cross sections for all three channels are negligibly small, but they begin to rise rapidly from 360 MeV/c to a maximum at about 400 MeV/c. The $\Sigma^-\pi^+\pi^0$ and $\Sigma^0\pi^+\pi^-$ cross sections show peaking near the energy required to form $\Lambda(1520)$. The $\Sigma^+\pi^-\pi^0$ cross section remains constant above 400 MeV/c, indicating background contributions above the $\Lambda(1520)$ region. The curves in Fig. 1 result from fits described below.

Even at the low momentum considered here there are a large number of possible spin and angular momentum couplings in a three-body final state. The low statistics available here do not allow an independent detailed analysis of these events. Therefore, we take as a guide to the interpretation of the mass and angular distributions of the $\Sigma\pi\pi$ events the detailed analysis of the $\Lambda\pi^+\pi^-$ final state from the same exposure.[1] The main conclusion from that analysis (described in more detail below) is that the $\Lambda\pi\pi$ final state is dominated by the reaction sequence $K^-p \rightarrow \Lambda(1520)$ $\rightarrow \Sigma(1385)\pi \rightarrow \Lambda\pi^+\pi^-$. This result suggests the presence of $\Sigma(1385)$ production in the $\Sigma\pi\pi$ final states. The branching fraction $\Gamma[\Sigma(1385) \rightarrow \Sigma^+\pi^0]/$ $\Gamma[\Sigma(1385) \rightarrow \Lambda\pi^+]$ is about 5%.[4] The ratio of $\Sigma\pi\pi/$ $\Lambda\pi\pi$ events that we observe is a similar percentage. Thus from these rough numbers and our understanding of the $\Lambda\pi\pi$ we expect that the $\Sigma(1385)$ is making a significant contribution to the $\Sigma\pi\pi$ final states.

The Dalitz plots for the $\Sigma\pi\pi$ events show no definite structure. At the energies considered here only the lower edges of $\Sigma(1385)$ bands overlap the kinematic region. Figure 2 shows the $\Lambda\pi\pi$ and $\Sigma\pi\pi$ Dalitz-plot boundaries at 395 MeV/c and the positions of M^2 and $(M - \Gamma)^2$ for the $\Sigma(1385)$. Hence isobar-model predictions for the Dalitz-plot distributions are very sensitive to the masses and widths of the various charged Y^*'s and their interference. The uncertainty in these widths and masses and the low statistics of our sample preclude any determination from the Dalitz plots of the amount of $\Sigma(1385)$ present. The possibility of interferences with background further complicates the analysis.

The angular distribution of the hyperon with respect to the beam in the over-all center of mass has traditionally been used to search for the presence of the production and decay of the $\Lambda(1520)$ into $\Sigma(1385)\pi$. Figures 3(a)–3(c) show this distribution for the data between 380 and 410 MeV/c. The curves over the data are the results of a Monte Carlo prediction of the shape, using the $\Sigma(1385)$ production amplitudes that were

found to fit the $\Lambda\pi\pi$ final states. The agreement is good and this is evidence that the same amplitudes account for the $\Sigma\pi\pi$ data. However, the data are also nearly consistent with isotropy. Isotropic distributions are expected from three-body phase space, which is $a priori$ not an unreasonable model at these low energies. Distributions that do show more structure both in the data and predictions are shown in Figs. 4(a)–4(c). This is the cosine of the angle between the incident beam and the normal to the three-particle plane in the over-all center-of-mass system. Three-body phase space predicts constant distributions. The data agree more closely with the predictions of $\Sigma(1385)$ production. The χ^2's for the curves in Figs. 4(a)–4(c) are 9.4, 12.4, and 7.9, respectively. The χ^2's for isotropic distributions are 37.5, 25.7, and 11.5. We conclude that the $\Sigma\pi\pi$ data are consistent with dominance by the reaction sequence $K^-p \rightarrow \Lambda(1520) \rightarrow \Sigma(1385)\pi$ $\rightarrow \Sigma\pi\pi$. We will $assume$ in the remainder of this analysis that the same $\Sigma(1385)$ production amplitudes that contribute to the $\Lambda\pi\pi$ final state also account for the $\Sigma\pi\pi$ data.

IV. COMPARISON OF $\Sigma\pi\pi$ AND $\Lambda\pi\pi$ CROSS SECTIONS

A comparison of the $\Sigma\pi\pi$ and $\Lambda\pi\pi$ final states must take into account the different amplitudes for the decay of the $\Sigma(1385)$ and the different amount of phase space available to the final states. The amplitudes used for this comparison are of the same form as those used in the analysis of the
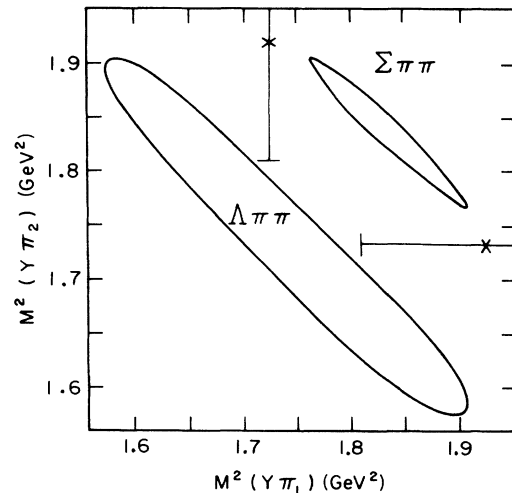

FIG. 2. Diagram showing the boundaries of the Dalitz plots for $\Lambda\pi\pi$ and $\Sigma\pi\pi$. The symbol X indicates M^2 and $(M - \Gamma)^2$ for the $\Sigma(1385)$.

$\Lambda \pi^+ \pi^-$ final state.[1] That study consisted of an energy-independent partial-wave analysis based on the isobar model of Deler and Valladas.[5] The isobar model describes the three-body final state in terms of the production of a single particle and an isobar and the subsequent decay of the isobar. Thus the amplitude for the three-body final state is written as a sum of amplitudes each of which describes the production of an isobar in a particular angular momentum state L through an initial $K^- p$ state of definte spin-parity J^P. For example,

$$A^{J^P, L}(K^- p \rightarrow \Sigma^0 \pi^+ \pi^-) = C_1 f_1^{J^P, L} T_1 + C_2 f_2^{J^P, L} T_2,$$

(6)

where 1 (2) refers to the coupling of the first (second) pion to the hyperon to form the isobar. The f's are functions of the angular variables, spins, and angular momenta of the final state, and their detailed form is described in Ref. 1. C_1 and C_2 are Clebsch-Gordan coefficients for the production and decay of the $\Sigma(1385)$.[6] The T's are Breit-Wigner forms describing the decay of the $\Sigma(1385)$. For the $\Sigma^0 \pi^+ \pi^-$ example chosen above,
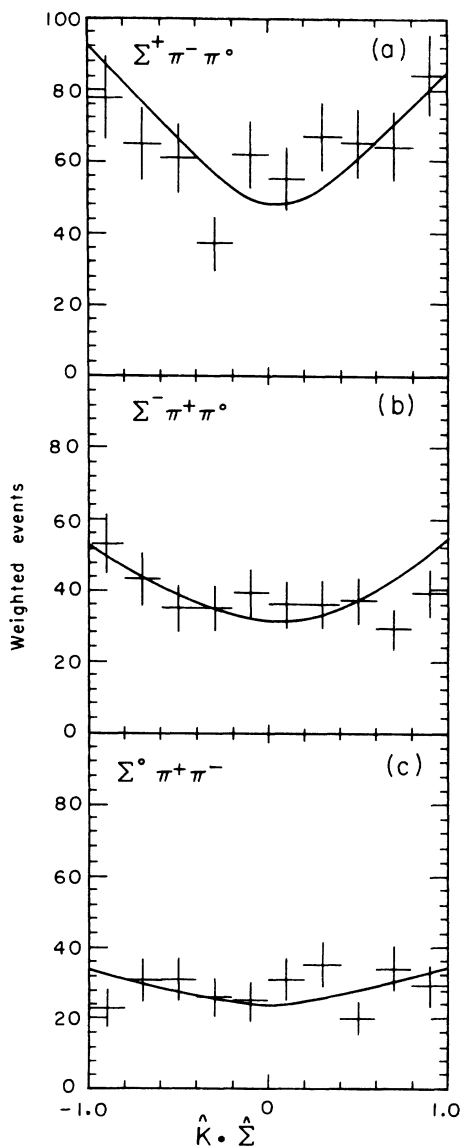
FIG. 3. The distribution of the cosine of the angle between the Σ and the incident beam in the $K^- p$ center-of-mass system for (a) $\Sigma^+ \pi^- \pi^0$, (b) $\Sigma^- \pi^+ \pi^0$, and (c) $\Sigma^0 \pi^+ \pi^-$. The curves are the predictions of the isobar model described in the text.
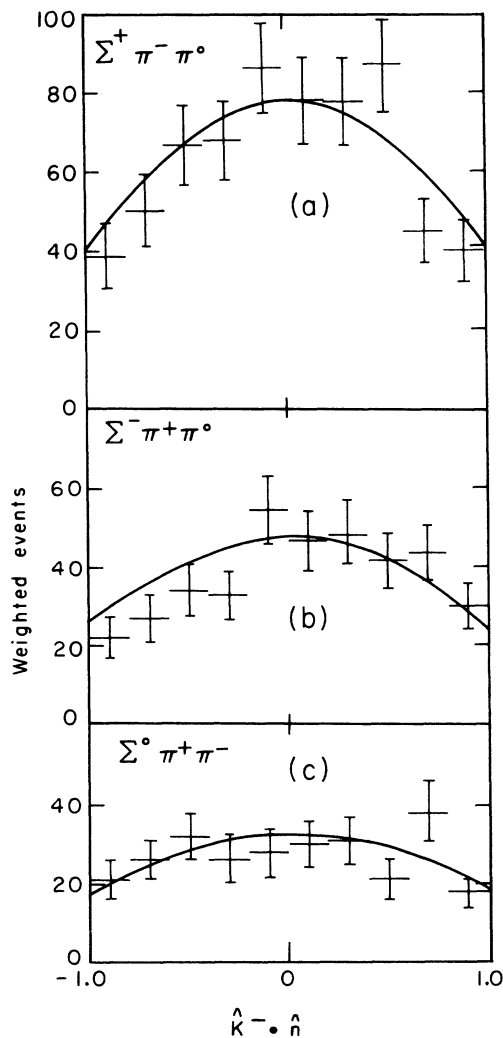
FIG. 4. The distribution of the cosine of the angle between the normal to the three-body plane and the incident beam in the $K^- p$ center-of-mass system for (a) $\Sigma^+ \pi^- \pi^0$, (b) $\Sigma^- \pi^+ \pi^0$, and (c) $\Sigma^0 \pi^+ \pi^-$. The curves are predictions from the isobar model discussed in the text.
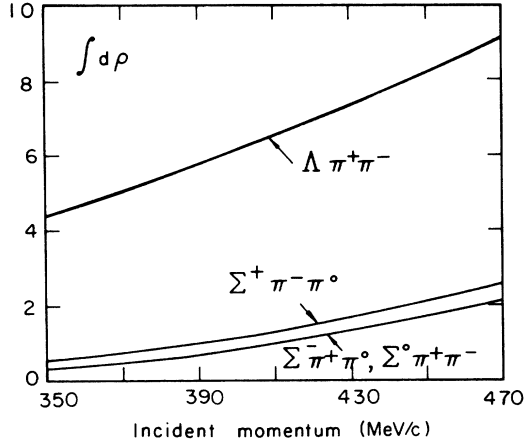
FIG. 5. The integral of three-body phase space as a function of incident momentum for $\Lambda\pi^+\pi^-$, $\Sigma^+\pi^-\pi^0$, $\Sigma^-\pi^+\pi^0$, and $\Sigma^0\pi^+\pi^-$.
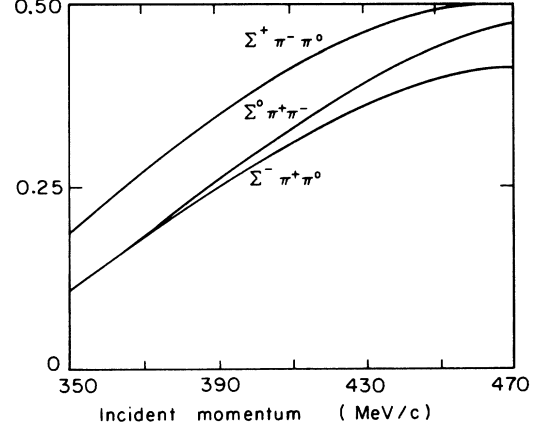

FIG. 6. The ratios of the integrals of the isobar-model amplitude Y^*DS03 squared over the three-body phase space as a function of incident momentum for various $\Sigma\pi\pi/\Lambda\pi\pi$.

$$T_{1,2} = \frac{(\gamma_\pm/p_\pm)^{1/2}}{m_{\Sigma\pi\pm} - m_{Y*\pm} - (\frac{1}{2}i\Gamma_T)}, \tag{7}$$

where

$$\gamma_\pm = \frac{\Gamma_{Y*\pm \to \Sigma^0\pi^\pm}(p_\pm)}{\Gamma_{Y*+ \to \Sigma^0\pi^+}(p_R)}$$

and

$$\Gamma(p) \propto \frac{p^3}{1 + r^2p^2}$$

The quantity $m_{\Sigma\pi}$ is the invariant mass of the $\Sigma\pi$ system and $p_\pm$ is the momentum of the $\Sigma^\pm$ in the $Y^{*\pm}$ rest frame. The width $\gamma_\pm$ is divided by $p_\pm$ to remove the isobar phase space, which is regained upon squaring the amplitude and integrating it over three-body phase space.

The quantities m_{Y*} and Γ_T are the mass and total width of the $\Sigma(1385)$. The total width is

taken to be 40 MeV, and the radius of interaction r to be 1 F. p_R is the value of the decay momentum when $m_{\Sigma\pi} = m_{Y*}$. The width for one of the channels is chosen for the normalization.

The values of L and J^P used in this comparison are based on the analysis of the $\Lambda\pi^+\pi^-$. There the data between 350 and 470 MeV/c were fitted with a sum of six amplitudes. Four of these amplitudes invlove the production of $\Sigma(1385)$ and its subsequent decay into Λ and π. The remaining two amplitudes couple the two pions in an $I = 0$ S-wave dipion state, which then decays. The $\Lambda\pi^+\pi^-$ cross section is dominated by the amplitude corresponding to the $I = 0$, $J^P = \frac{3}{2}^-$ production of a $\Sigma(1385)$ and π (denoted Y^* $DS03$),[7] corresponding to reaction sequence (1). Of the three remaining $\Sigma(1385)$ isobar amplitudes, only one contributes significantly to the cross section. This is the $I = 0$ P-wave production of the $\Sigma(1385)$

TABLE II. Measured cross sections (mb) for $\Sigma^+\pi^-\pi^0$, $\Sigma^-\pi^+\pi^0$, and $\Sigma^0\pi^+\pi^-$. The last two columns are the Y^*DS03 and Y^*PP01 contributions to the measured $\Lambda\pi^+\pi^-$ cross section (see Ref. 1).

Momentum interval (MeV/c)	$\sigma(\Sigma^+\pi^-\pi^0)$	$\sigma(\Sigma^-\pi^+\pi^0)$	$\sigma(\Sigma^0\pi^+\pi^-)$	$\sigma(DS03)$	$\sigma(PP01)$
350–360	0.015 ± 0.009	0.000 ± 0.003	0.005 ± 0.005	0.23 ± 0.02	0.03 ± 0.03
360–370	0.041 ± 0.009	0.030 ± 0.007	0.023 ± 0.007	0.72 ± 0.04	0.08 ± 0.03
370–380	0.075 ± 0.010	0.050 ± 0.007	0.039 ± 0.008	1.13 ± 0.04	0.06 ± 0.02
380–390	0.120 ± 0.012	0.080 ± 0.008	0.089 ± 0.011	1.84 ± 0.06	0.18 ± 0.04
390–400	0.151 ± 0.015	0.080 ± 0.009	0.096 ± 0.012	1.96 ± 0.06	0.13 ± 0.04
400–410	0.152 ± 0.016	0.087 ± 0.010	0.106 ± 0.015	1.64 ± 0.06	0.11 ± 0.04
410–420	0.142 ± 0.020	0.072 ± 0.012	0.059 ± 0.014	1.10 ± 0.06	0.14 ± 0.06
420–430	0.128 ± 0.031	0.032 ± 0.012	0.032 ± 0.016	0.50 ± 0.04	0.13 ± 0.07
430–440	0.159 ± 0.040	0.075 ± 0.023	0.051 ± 0.023		
440–450	0.143 ± 0.038	0.058 ± 0.021	0.057 ± 0.030	0.38 ± 0.04	0.19 ± 0.10
450–460	0.066 ± 0.039	0.085 ± 0.039	0.041 ± 0.030		

(Y^*PP01), which accounts for 5% of the cross sec-
tion in the region of the resonance. The major
background term is the $I=0$, $J^P = \frac{1}{2}^+$ production
of the S-wave dipion (σ $PS01$).

Since we cannot relate the σ amplitudes corre-
sponding to $\sigma\Lambda$ production to some corresponding
amplitudes for $\sigma\Sigma$, we have not used these ampli-
tudes to understand the background in $\Sigma\pi\pi$. The
two Y^* production amplitudes $DS03$ and $PP01$
have been used to describe the $\Sigma\pi/\Lambda\pi$ branching
ratio of the $\Sigma(1385)$. For example, for one am-
plitude the ratio of the contributions to the mea-
sured cross sections is

$$\frac{\sigma(\Sigma^0\pi^+\pi^-)}{\sigma(\Lambda\pi^+\pi^-)} = \frac{\int_{\Sigma\pi\pi}|A_{\Sigma\pi\pi}|^2 \, d\rho \, 2\Gamma_{Y*+\to\Sigma0\pi+}(p_R)}{\int_{\Lambda\pi\pi}|A_{\Lambda\pi\pi}|^2 \, d\rho \, \Gamma_{Y*+\to\Lambda\pi+}(p_R)} \, .$$

$$(8)$$

The amplitude A for each final state is given by
Eqs. (6) and (7) with the appropriate masses and
Clebsch-Gordan coefficients.[8] The integrals over
$d\rho$ are over the three-body phase space. The
ratio of this phase space for $\Sigma^0\pi^+\pi^-$ to that for
$\Lambda\pi^+\pi^-$ is about 0.13 at 395 MeV/c (Fig. 5). The
greater penetration of the $\Sigma(1385)$ bands into the
$\Sigma\pi\pi$ Dalitz plot and the different Clebsch-Gordan
coefficients increases the ratio of the integrals
over the matrix elements to about 0.28. The
ratio of the integrals for the $DS03$ amplitude is
shown as a function of incident momentum in Fig.
6. Similar ratios have been calculated for the
$PP01$ amplitude. Since only the $DS03$ and $PP01$
were significant in the final state, we have only
included these in describing the $\Sigma\pi\pi$. Since they
correspond to different total J^P there is no con-
tribution to the cross section from the interfer-
ence between these waves.

The cross sections in Fig. 1 have been fitted
to the sum of three terms: a contribution from
the $\Lambda(1520)$, the $DS03$ wave; a fixed fraction of
$PP01$ wave; and a phase-space term for the back-
ground.

$$\sigma = \frac{4\pi\lambda^2 x_e x_r}{\epsilon^2 + 1} + \sigma_{\Sigma\pi\pi}(PP01) + B\int_{\Sigma\pi\pi} d\rho \, ,$$

where $\epsilon = (E - m_{1520})/(\Gamma_T/2)$, and x_e, the elasticity
of the $\Lambda(1520)$, is 0.46. The energy dependence
of the cross section from $PP01$ is predicted by
using Eq. (8) and the contribution of each wave
to the $\Lambda\pi^+\pi^-$ cross section from Ref. 1 (columns
4 and 5 of Table II). The branching fraction x_r
and the amount of background B were varied in
a χ^2 fit. The resulting curves are plotted over
the data in Figs. 1(a)–1(c). No background is re-
quired for the $\Sigma^-\pi^+\pi^0$ and $\Sigma^0\pi^-\pi^-$ channels. The
χ^2 for the $\Sigma^+\pi^-\pi^-$ channels is improved by the
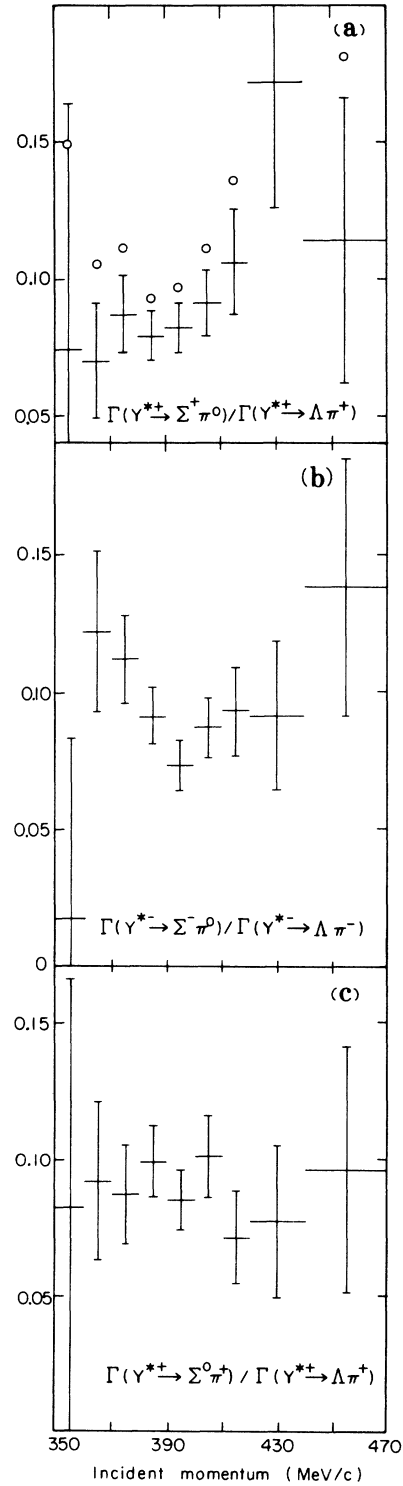phase-space background, shown as a dashed line

FIG. 7. The $\Sigma\pi/\Lambda\pi$ branching ratio for the Σ (1385)
measured at nine different incident momenta for the
charge channels indicated. The circles in (a) show the
branching ratio before the background subtraction
described in the text.

in Fig. 1(a). The χ^2's for the three cross sections are 4.9, 17.1, and 10.8, respectively. The branching fractions into the charged channels $\Sigma^+\pi^-\pi^0$, $\Sigma^-\pi^+\pi^0$, and $\Sigma^0\pi^+\pi^-$ are 0.0034 ± 0.0004, 0.0024 ± 0.0003, and 0.0027 ± 0.0003, respectively. Thus the total branching fraction of the $\Lambda(1520)$ into $\Sigma\pi\pi$ is 0.0085 ± 0.0006.

Finally, as a consistency check, we use the measured $\Sigma\pi\pi$ and $\Lambda\pi\pi$ cross sections and Eq. (8) to calculate the branching ratio BR of the $\Sigma(1385)$. The branching ratios calculated at each incident momentum are shown in Figs. 7(a)–7(c). The cross sections used for the $\Sigma^+\pi^-\pi^0$ channel were the measured cross sections reduced by the amount of phase-space background found in the above fits. The circles are the branching ratios without this background subtraction. The branching ratios are found to be independent of momentum. Taking the weighted mean of the nine values for each channel yields

$$\alpha = \frac{\Gamma(Y^{*+} \rightarrow \Sigma^+\pi^0)}{\Gamma(Y^{*+} \rightarrow \Lambda\pi^+)} = 0.085 \pm 0.005,$$

$$\beta = \frac{\Gamma(Y^{*-} \rightarrow \Sigma^-\pi^0)}{\Gamma(Y^{*-} \rightarrow \Lambda\pi^-)} = 0.089 \pm 0.005,$$

$$\gamma = \frac{\Gamma(Y^{*+} \rightarrow \Sigma^0\pi^+)}{\Gamma(Y^{*+} \rightarrow \Lambda\pi^+)} = 0.089 \pm 0.006.$$

From phase-space considerations the ratios α/γ and γ/β should be 1.17 and 0.97, respectively. Our measured values give 0.96 ± 0.08 and 1.00 ± 0.09. The fraction from the $\Sigma^+\pi^-\pi^0$ final state is lower than expected. Without the background subtraction applied to this channel the ratio α/γ is consistent with phase space.

The total $\Sigma\pi$ to $\Lambda\pi$ branching ratio is given by

$$\frac{\Gamma(Y^{*+} \rightarrow \Sigma^0\pi^+)(1 + 1.17)}{\Gamma(Y^{*+} \rightarrow \Lambda\pi^+)} = 0.193 \pm 0.013,$$

$$\frac{\Gamma(Y^{*-} \rightarrow \Sigma^-\pi^0)(1 + 0.96)}{\Gamma(Y^{*-} \rightarrow \Lambda\pi^-)} = 0.174 \pm 0.010.$$

Including an estimation of the systematic errors, we conclude

$$\frac{\Gamma(Y^* \rightarrow \Sigma\pi)}{\Gamma(Y^* \rightarrow \Lambda\pi)} = 0.18 \pm 0.04.$$

This is higher than the world average value 0.125 ± 0.021.[4] The prediction from SU(3) varies from 0.14 to 0.20 depending on the radius of interaction chosen for the barrier factor.

Variation of the input parameters to the calculation of the integrals does not have a large effect on these results. For example, changing the total width of the $\Sigma(1385)$ from 40 to 35 MeV reduces the branching ratio by 6% of its value. Our results do of course depend strongly on our assumptions that the $\Sigma\pi\pi$ channels are dominated by reaction sequence (2) and that there are no large interferences between this contribution and background. Without these assumptions our value for the branching ratio represents an upper limit, since the $\Sigma\pi\pi$ distributions are nearly consistent with phase space.

*Work done under the auspices of the U. S. Atomic Energy Commission.

[1]T. S. Mast, M. Alston-Garnjost, R. O. Bangerter, A. Barbaro-Galtieri, F. T. Solmitz, and R. D. Tripp, Phys. Rev. D 7, 5 (1973).

[2]S. E. Derenzo and R. H. Hildebrand, LBL Report No. UCRL-18638, 1968 (unpublished).

[3]The Σ track length is usually too short to give a useful momentum measurement. Otherwise the $\Sigma^\pm\pi^\mp\pi^0$ events would have two constraints, and the $\Sigma^\pm\pi^\mp$ events five constraints.

[4]Particle Data Group, Phys. Lett. 39B, 1 (1972).

[5]B. Deler and G. Valladas, Nuovo Cimento 45A, 559 (1966).

[6]The relative sign of C_1 and C_2 is positive for the $\Lambda\pi\pi$ and negative for the $\Sigma\pi\pi$ channels. This difference in the sign of the interference between the two possible Y^*'s

is critical for the correct prediction of the observed angular distributions (Figs. 3 and 4). C_1 and C_2 are equal in magnitude for all the channels considered and they are smaller by $\sqrt{2}$ for the $\Sigma\pi\pi$ final states compared to $\Lambda\pi\pi$.

[7]The notation here is $LL'I2J$, where L and L' refer to the orbital angular momentum for the incoming K^-p system and the outgoing quasi-two-body system (Y^* or σ), respectively, I is the isotopic spin of the $Y\pi\pi$ system, and J is the total angular momentum of the $Y\pi\pi$ system.

[8]The factor 2 in Eq. (8) comes from a redundancy in the amplitude definitions [Eqs. (6) and (7)]. The Clebsch-Gordan coefficients include $1/\sqrt{2}$ to account for the $\Sigma(1385)$ decay into a charged state; however, the partial width used in the Breit-Wigner factor is for the charged final state.